

PSFC/RR-10-11

**Effect of Wall Reflections on Hot Electron Temperature
from ECE Diagnostics in LDX**

D.J. Charles* and P. Woskov

* University of South Florida

September 2010

**Plasma Science and Fusion Center
Massachusetts Institute of Technology
Cambridge MA 02139 USA**

This work was supported by the U.S. Department of Energy. Reproduction, translation, publication, use and disposal, in whole or in part, by or for the United States government is permitted.

Effect of Wall Reflections on Hot Electron Temperature from ECE Diagnostics in LDX

Daniel Charles

Advisor: Dr. Paul Woskov

Background

The Levitated Dipole Experiment (LDX) at MIT uses a floating donut-shaped superconducting magnet to study the confinement of plasma in a dipole magnetic field. LDX created its first plasma in 2004 and first levitated its superconducting magnet in 2007. Compared to the more popular tokamak, first used to create plasma in the 1960s, LDX is a relatively new device. Despite this, there is speculation that the magnetic field configuration in LDX may prove to be superior to that of the tokamak, with respect to the eventual goal of nuclear fusion.^[1]

Three superconducting magnetic coils are used in LDX: the C-coil, the F-coil, and the L-coil. The experiment's vacuum chamber, which measures approximately 3.0 m tall and 5.0 m in diameter, contains the floating magnetic coil, or the "F-coil" (see Figure 1). The F-coil, which weighs approximately 550 kg, can be held up by metal supports, but since it was first levitated in November 2007, most experiments levitate the F-coil. In an experimental campaign, the charging coil (the "C-coil,"

located beneath the vacuum chamber) induces a current in the F-coil. The charged F-coil is lifted up mechanically, and the levitation coil ("L-coil," located on top of the vacuum chamber) creates a magnetic field to suspend the F-coil in place. The final magnetic field is a combination of the fields generated by both the L-coil and the F-coil. In the region of interest (that is, regions within the chamber with closed field lines), the field is dominated by the field of the F-coil, which is roughly the shape of a dipole (see Figure 2). Note that Figure 2 is a cross-section of LDX; therefore, the "field lines" drawn are actually a cross section of the three-dimensional toroidal field surrounding the F-coil.

After using vacuum pumps to reduce the pressure in the chamber, small amounts of gas (typically deuterium or helium) are puffed in. Several microwave sources (two 2.45 GHz magnetrons, a 6.4 GHz klystron, a 10.5 GHz klystron, and a 28 GHz gyrotron, with a total available power of 26.9 kW) ionize the gas.

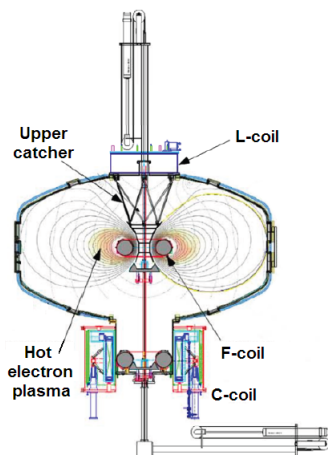


Figure 1: A cross section of the Levitated Dipole Experiment (LDX). Based on Figure 3-3.^[2]

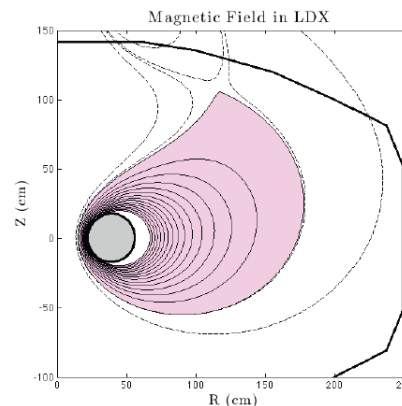


Figure 2: The magnetic field surrounding the F-coil in LDX. The pink region contains all of the closed field lines that the plasma can move along. The Z axis is the vertical distance from the center of LDX, and the R axis is the horizontal distance from the center. Source: Figure 3-6.^[2]

This generates and sustains plasma through a process known as electron cyclotron resonance heating (ECRH).

A charged particle confined in a magnetic field will travel unobstructed if its velocity is parallel to a field line, but if the particle has a velocity component perpendicular to the field line, it will experience a Lorentz force ($\vec{F} = q\vec{v} \times \vec{B}$). This causes the particle to undergo helical motion, rotating about the field line at a frequency called the cyclotron frequency ($\omega_c = qB/m$).^[3] Particles rotating about a field line at the cyclotron frequency ω_c will readily absorb and emit radiation at that frequency or its harmonics ($\omega_c, 2\omega_c, 3\omega_c, \text{etc. } \dots$). When the particles absorb radiation, the technique at work is known as ECRH; microwave radiation heats (that is, provides energy to) the charged particles (electrons) in LDX.

In LDX, we can consider the electrons of the plasma as belonging to two groups, “warm” electrons and “hot” electrons, which can each be modeled by a Maxwellian energy distribution. The hot (higher energy) electrons have been previously estimated to have a temperature greater than 50 keV (580 million Kelvin), perhaps as high as 100 to 250 keV (1.15 to 2.90 billion Kelvin).^[4] Most of the electrons are warm electrons, which have significantly lower temperatures. Figure 1 shows the region occupied by the hot electrons, which is the electron group that we will focus on in this paper.

Also, note that the rotating electrons in LDX are accelerating charges. Therefore, like all accelerating charges, they emit radiation while rotating about a magnetic field line. This radiation, known as electron cyclotron emission (ECE), is one of the plasma diagnostic measurements in LDX, and is the main focus of this paper. Two radiometers located near the top of the chamber, one at 110 GHz and one at 137 GHz, measure ECE emitted by the plasma. The signals from these radiometers can be used to find the temperature of the hot electrons.

Modeling of ratio versus temperature

In order to determine the hot electron temperature, a model must relate the signal to the temperature. A previous model assumed that reflection of radiation off of the chamber walls was negligible. This model used a direct view of the signal, tracing the view of the radiometer along the field line with the strongest emission. Because the plasma density falls off as r^{-4} , any emission from field lines distant from the peak is considered negligible. This assumption is used in both the previous and current models. The model described in this paper considers reflections off of the chamber walls, assuming that all radiation will eventually strike the receiver. Emission is considered from the entire field line at all angles. The most accurate model is likely a combination of these two models, using reflectivity factors for the emission that is not in direct view.

It is important to note that both of these models are two-dimensional, looking only at the emission from a cross section of LDX. The actual experiment is three-dimensional and thus much more complicated to model. Future work may involve three-dimensional modeling of ECE in LDX, but the present two-dimensional model should suffice as a first approximation.

Both models were evaluated with MATLAB programs, based on Equation (2) from A. Nassri’s 1988 paper:^[5]

$$\alpha_\omega(\theta, \bar{\omega}, \mu) = \frac{\omega_p^2}{c\omega_c} \frac{\pi\mu^2}{2K_2(\mu)} \sum_{m=[\bar{\omega} \sin \theta]}^{\infty} \quad (1)$$

$$m^{-1} \int_{\tau_1}^{\tau_2} \left[\sin^{-2} \theta \left(\cos \theta - \frac{v_{||}}{c} \right)^2 J_m^2 \times \left(\frac{\bar{\omega} w_{||}^{1/2} \sin \theta}{u_{||}} \right) + \frac{w_{||}}{c^2} J_m^2 \left(\frac{\bar{\omega} w_{||}^{1/2} \sin \theta}{u_{||}} \right) \right] \times u_{||}^{-4} \exp \left(-\frac{\mu c}{u_{||}} \right) dv_{||}$$

where $\alpha_\omega(\theta, \bar{\omega}, \mu)$ is the absorption coefficient

of the plasma, $\omega = 2\pi f$ is the radiation frequency, θ is the angle between the wavevector \vec{k} and the magnetic field line \vec{B} , $\bar{\omega} = \omega/\omega_c$, $\mu = m_0c^2/kT$ is the temperature-dependent term, and the plasma frequency ω_p can be expressed as follows:^[3]

$$\omega_p = \left(\frac{n_0 e^2}{\epsilon_0 m} \right)^{1/2}$$

Note that the plasma frequency ω_p depends on the electron density n_0 . The hot electron density is not known, so the best way to handle it theoretically is to eliminate the ω_p term. By taking the ratio of α at two frequencies (in our case, 137 GHz and 110 GHz), the constant term $\omega_p^2/(c\omega_c)$ drops out of Equation (1). The ultimate goal then is to find a relationship between the ratio of ECE signals to the temperature.

Because $\bar{\omega}$ expresses the frequency as a multiple of ω_c , it is often referred to as the harmonic number. To clarify its meaning, let us evaluate the numerator and denominator:

$$\begin{aligned} \bar{\omega}_{min} &= \frac{\omega}{\omega_c} \\ &= \frac{2\pi f}{\frac{qB}{m}} \\ &= \frac{2\pi m}{q} \frac{f}{B} \end{aligned}$$

Aside from constants, $\bar{\omega}$ depends only on the frequency of the ECE (which is equal to the frequency of the radiometer used to measure it) and the magnetic field at the location where the ECE is emitted.

The following are the steps used to evaluate this equation in MATLAB for the new model with reflections:

Evaluate integration limits τ_1 and τ_2 → Evaluate integrands → Evaluate integral with Simpson's rule → Sum over m

Each step of the flowchart is a separate MATLAB program, and each program calls on pre-

vious programs to perform a calculation. The program that sums over m calls on a separate program to evaluate the integral for that value of m . That program in turn must call on other programs to determine the integrands and the integration limits. Since an infinite sum can't be computed numerically, the sum over m is only performed until additional terms become negligible (specifically, when the next additional term becomes less than 1/10,000th of the sum thus far). An upper limit of $m = 200$ was set to avoid an infinite loop.

Once Eq. 1 is evaluated, two more integrals are performed. First the equation is evaluated from $\theta = 1$ degree to 89 degrees in increments of 4 degrees. The curve of $\alpha(\theta, \bar{\omega}, \mu)$ versus θ is then integrated with the trapezoidal rule. It was found that 4-degree increments are sufficient for an accurate integration; running with 0.1-degree increments produced a nearly identical result, despite running forty times longer. After integrating over θ , the function $\alpha(\bar{\omega}, \mu)$ is evaluated from $\bar{\omega} = \frac{1}{2000}$ to 12 in increments of $\frac{1}{2000}$. The curve of $\alpha(\bar{\omega}, \mu)$ versus $\bar{\omega}$ is then integrated with the trapezoidal rule, giving the desired result of absorption for a given μ (which is proportional to the emission for a given temperature).

For a given temperature, the only difference between the different cases in this model

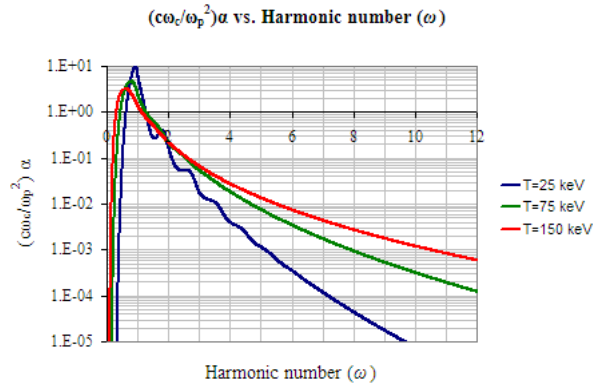


Figure 3: Plot of angle-integrated absorption coefficient (α) divided by the constant term ($\omega_p^2/(c\omega_c)$) versus harmonic number ($\bar{\omega}$) for $T = 25, 75,$ and 150 keV.

is the range of $\bar{\omega}$ over which we integrate. (See Figure 3 for plots of α versus $\bar{\omega}$, normalized for the constant term.) In our model, all cases go up to $\bar{\omega} = 12$; any emission at higher frequencies is negligible. The lower limit depends on the frequency of the radiometer and how high of a magnetic field we wish to examine. In our model that considers all possible reflections, we use the highest value of the magnetic field along the field line.

When determining the maximum value of $|\vec{B}|$ (and therefore the minimum value of $\bar{\omega}$), we must consider which field line should be examined, because different field lines have different maximum values of $|\vec{B}|$. As stated earlier, we are examining only emission at the plasma density peak, assuming all other emission is negligible. However, we do not know the exact radial position of the density peak (that is, the L -value; in Figure 2, this corresponds to the R coordinate). For most of our calculations, we estimate that the peak is at $L = 75$ cm; however, we have also examined the cases where $L = 70$ cm and $L = 80$ cm.

For the case of $L = 75$ cm, the maximum value of $|\vec{B}|$ is 3.06 T. (This maximum occurs inside the central hole of the F-coil, along the midplane; that is, at $Z = 0$.) Using this value for the 137 GHz radiometer,

$$\begin{aligned}\bar{\omega}_{min} &= \frac{2\pi m}{q} \frac{f}{B} \\ &= \frac{2\pi(9.109 \times 10^{-31} \text{ kg})}{1.602 \times 10^{-19} \text{ C}} \frac{137 \times 10^9 \text{ Hz}}{3.06 \text{ T}} \\ &\approx 1.60\end{aligned}$$

Using the same value for $|\vec{B}|$ and $f = 110$ GHz, $\bar{\omega}_{min} \approx 1.28$ for the other receiver.

The resulting value from integrating α over $\bar{\omega}$ is proportional to the electron cyclotron emission at a given temperature and a frequency corresponding to one of the radiometers (110 GHz or 137 GHz). By taking ratios of these values (137 GHz emission divided by 110 GHz emission) over many temperatures from 3

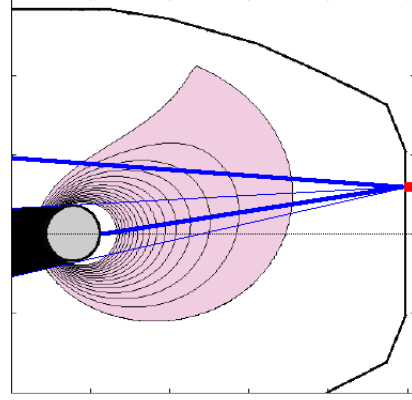


Figure 4: Case 2 considers reflections but only examines emission from regions in view of the radiometer, which is located at the red square on the right. The heavy blue lines show the field-of-view, where the signal drops to $1/e^2$. The region in black, shadowed by the F-coil, is out of view. Based on Figure 3-6, p. 73.^[2]

keV to 300 keV, we obtain a curve of signal ratio versus temperature. (Eighteen values of temperature were used to generate these calibration curves: 3, 5, 7.5, 10, 15, 20, 25, 31, 37.5, 43, 50, 60, 75, 100, 150, 200, 250, and 300 keV.) Using this calibration curve, the experimentally observed signal ratio can be converted to hot electron temperature.

Four main cases are examined in this paper. Case 1 examines reflections from all frequencies along the field line with the strongest emission. Case 2 is the same as Case 1, except it neglects emission from the region shadowed by the F-coil. (See Figure 4.) Case 3 corresponds to the previous model, examining the direct view from the antenna along the field line. Case 4 examines a combination of the previous three cases, with reflectivity factors for the cases that integrate over θ . Table 1 lists the $\bar{\omega}_{min}$ values used for Cases 1 and 2.

When constructing Case 4, we assumed two different reflectivity factors for the different regions of reflections. Case 1 - Case 2 (the emission from the shadowed region) was given a reflectivity factor r_1 , and Case 2 (everything except the emission from the shadowed region) was given a reflectivity factor r_2 . Written ex-

Case	Radiometer	$L = 70$	$L = 75$	$L = 80$
1	110 GHz	1.246	1.285	1.319
	137 GHz	1.552	1.600	1.642
2	110 GHz	1.952	1.968	1.988
	137 GHz	2.432	2.451	2.476

Table 1: List of $\bar{\omega}_{min}$ values for the different cases examined.

licitly, Case 4 was constructed as follows:

$$\text{Case 4} = \text{Case 3} + r_1 \times (\text{Case 1} - \text{Case 2}) + r_2 \times \text{Case 2} \quad (2)$$

It is important to note that this operation must be performed on the integrated absorption coefficients (α , after integrating over $\bar{\omega}$), and not on the ratios. The ratio is not physically meaningful; rather, it is the actual amount of emission that we must operate on.

Figure 5 shows the calibration curve obtained for Case 3 (direct view), and Figure 6 shows the calibration curve obtained for Case 1 (complete reflections). These curves are very differently shaped; the ratio increases from zero in the direct view case, but when reflections are considered, the ratio decreases first and then increases. This occurs because the radiometers is viewing further into the central hole, at the strong fundamental emission. As

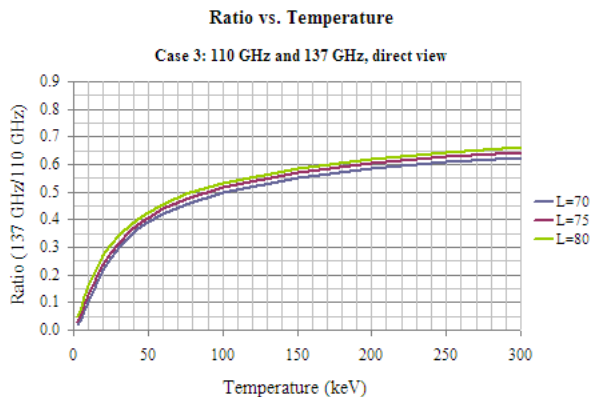


Figure 5: Calibration curve for Case 3, direct view with no reflections. The curve is plotted for three different assumptions of the plasma density peak: $L = 70$ cm, 75 cm, or 80 cm.

both radiometers view closer to the fundamental, the difference between them diminishes, and the ratio approaches 1. The next step is to examine the experimental data. If the data shows a “dipping” trend at the beginning similar to that seen in Figure 6, then the reflections are a major component of the emission; but if the data shows only an increase from zero, then the reflections are a small contribution to the total emission.

Experimental data: examining ratios

A typical experimental campaign at LDX lasts three days. On each day, around 30 to 40 plasma shots are taken. (A “shot” is a time period when data is taken. In most cases, this also means that the F-coil is levitated, the ECRH sources are turned on, and plasma is present.) A single shot typically lasts from ten to fifteen seconds. In that time, the data collection system takes around one million data points. MATLAB programs are used to examine the experimental data for the ratios of the ECE signals.

Experimental ECE data from LDX is measured in volts. The MATLAB programs perform several calculations to convert the units of the raw ECE data from volts into eV. First, to ensure that the baseline is zero, the mean of

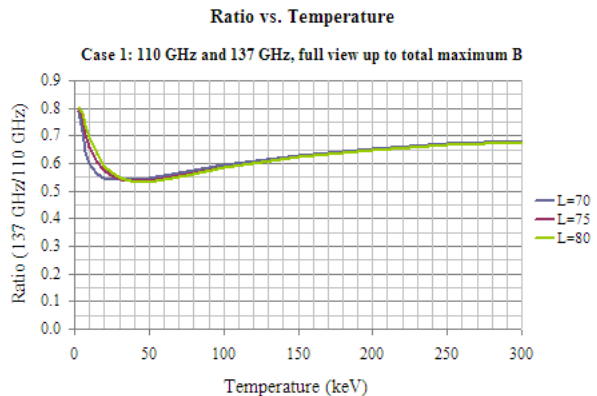


Figure 6: Calibration curve for Case 1, full view with complete reflection. The curve is plotted for three different assumptions of the plasma density peak: $L = 70$ cm, 75 cm, or 80 cm.

the first 14,000 data points is subtracted from the data. These points lie before the ECRH sources turn on, and therefore the mean of the ECE signal without the presence of plasma should be zero. If it isn't, the entire curve is likely shifted, so subtracting the mean will correct for this. Then the data is multiplied by -1000. This is done because the data is negative and in units of volts, but the calibration equation uses positive values in units of millivolts; multiplying by -1000 converts the data into the units needed for calibration.

The calibration equation for the radiometers is as follows:^[6]

$$KT_{in} = V_{out}(1 + \alpha V_{out}) \quad (3)$$

This equation is a best-fit line for calibrations performed before, during, and after an experimental campaign. T_{in} is the temperature of the signal input (in eV) and V_{out} is the voltage output of the radiometer (in mV). Calibration measurements are used to determine the value of the constant K , and past measurements give the value of the nonlinear term α . The MATLAB

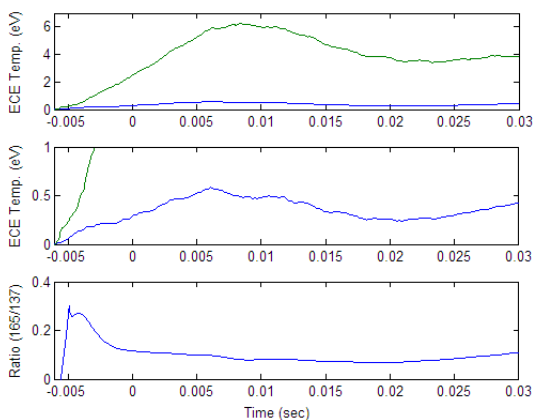


Figure 7: Plot of data from December 2008 showing an initial dip in the ratio. The plots go up to the first 30 milliseconds. The top two plots show the ECE; in green is the 137 GHz signal, and in blue is the 165 GHz signal. The y-axes are scaled differently to show the shape of each curve. The bottom plot shows the ratio of the two signals. Source: shot 81217017.

programs use this equation to convert the measured ECE signal from mV (V_{out}) to eV (T_{in}). The value of T_{in} is equivalent to the temperature of a corresponding blackbody that would give an output signal V_{out} if placed in front of the radiometer horn antenna.

While examining the experimental data with the radiometers at their present position, we did not observe an obvious downward trend of the ratio as the plasma was warming up. This indicates that the direct view is most likely the strongest component of the emission, with the addition of a smaller reflective component. However, in previous experiments, two radiometers (measuring at 165 GHz and 137 GHz at the time) were placed underneath LDX and looked directly into the central hole of the F-coil. This view looks into the shaded region in Figure 4, providing a direct view of the emission obscured from the present view. Indeed, some of the data from these experiments showed a downward trend within the first twenty milliseconds after plasma creation. Figure 7 is an example of a plot that shows this dip, from shot 81217017.

Various values of r_1 and r_2 were chosen when creating the calibration curve for Case 4. The actual values are not yet known, but it is

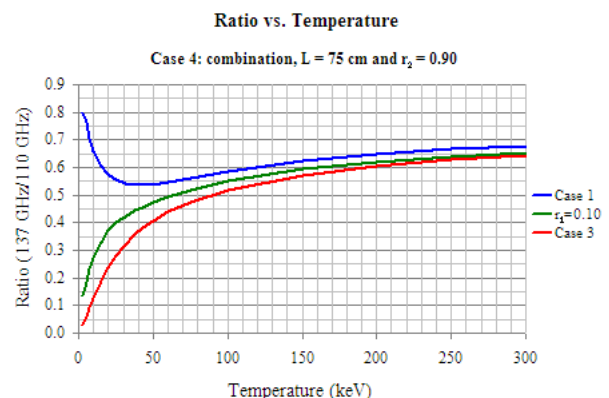


Figure 8: Calibration curve for Case 3 (direct view with no reflections — red), Case 1 (full view with complete reflections — blue), and Case 4 (combination with reflectivity factors — green), with $L = 75$ cm, $r_1 = 0.10$ and $r_2 = 0.90$.

informative to show what happens when different plausible values are chosen. A value of $r_1 = 0.10$, corresponding to the region shadowed by the F-coil, was chosen because it constitutes a smaller portion of the plasma. Its emission also has a more indirect path (requiring more wall reflections) to reach the radiometers. A value of $r_2 = 0.90$, corresponding to the region not shadowed by the F-coil, was chosen for the opposite reasons; it constitutes a larger portion of the plasma, and it would take fewer wall reflections to reach the radiometers. These values of r_1 and r_2 give a calibration curve for Case 4 that lies somewhere between those of Case 3 and Case 1. (See Figure 8.) The entire curve shifts upward from that of Case 3, especially at lower temperatures.

Different values of r_1 were plugged in to find the highest possible value before a dip appears at low temperatures. The exact value depends on the values of L and r_2 ; for example, for $L = 75$ cm and $r_2 = 0.50$, this value is $r_1 = 0.37$, but for $r_2 = 0.90$, it becomes $r_1 = 0.55$. For values of r_1 above this maximum value, the curve starts at a high ratio, has a minimum, and then rises again, much like the curve for Case 1. This sort of analysis can be used to set an upper value for r_1 , the reflectivity of the emission from the central hole of

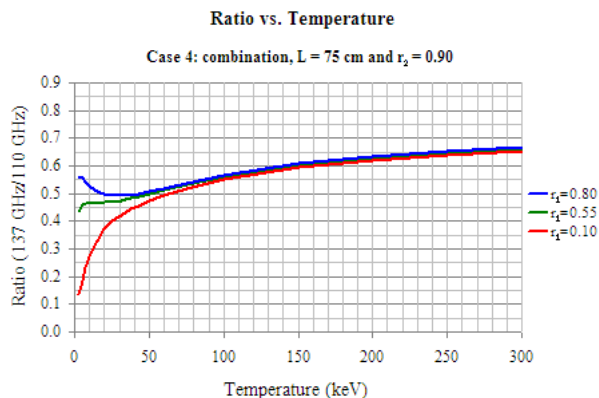


Figure 9: Calibration curve for Case 4, with $L = 75$ cm and $r_2 = 0.90$. The blue curve shows $r_1 = 0.80$, the green curve shows $r_1 = 0.55$ (the maximum value before the curve becomes double-valued), and the red curve shows $r_1 = 0.10$.

the F-coil. r_1 can't be any higher because the experimental data from the present view of the radiometers does not clearly show the ratio dip down and then increase as the plasma forms and begins to heat up. Figure 9 shows plots of the curve for Case 4 for three different values of r_1 .

Experimental data: examining temperatures

Using reasonable values of r_1 and r_2 ($r_1 = 0.10$ and $r_2 = 0.90$) and knowing the limit for r_1 ($r_1 \leq 0.55$ for $L = 75$ cm and $r_2 = 0.90$), the theoretical Case 4 curves were used to equate the ECE signal to hot electron temperature. Again, this was done with MATLAB programs. Two single-row matrices were inserted for a given case: a ratio matrix and a temperature matrix. These matrices are eighteen elements long, corresponding to the number of temperatures used to calculate the theoretical ratios. The n th element of the first matrix is the theoretical ratio calculated for the calibration curve, and the same element of the second matrix is the corresponding temperature. For each of the one million data points, the program reads in the experimental ratio and interpolates between our theoretical ratios to find the corresponding temperature. Figure 10 shows a plot of temperature

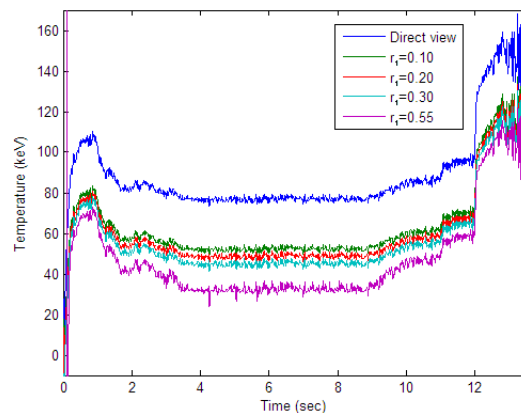


Figure 10: Temperature versus time for shot 100528008 for five different cases. The blue curve is Case 3, and the remaining curves are Case 4 for four different values of r_1 .

versus time for shot 100528008, using several different assumptions for the value of r_1 .

One factor that our model doesn't account for is the fill factor of the antenna. That is, it does not account for the fact that the plasma responsible for ECE does not completely fill the field of view of the radiometer. Consider, for example, if a radiometer views two separate objects: one at $T = 100$ keV that only fills 10% of the field of view, and one at $T = 10$ keV that fills the entire field of view. In both cases, the radiometer would give the same voltage output, suggesting that $T_{\text{in}} = 10$ keV. If this fill factor is not accounted for, then our conversions would show that the signal of any source that does not fill the field of view is too low.

The fill factor is the percentage of the field of view that is occupied by the signal from the source. Expressed another way, it is the ratio of the area of the source to the area of the field of view:

$$F = \frac{A_{\text{plasma}}}{A_{\text{view}}}$$

We chose to approximate A_{view} (the area of the field of view) as a circle whose radius is the beam's half-width, and A_{plasma} (the area of the plasma) as a thin rectangular strip across the diameter of the circle. (See Figure 11.) The equation for the half-width is^[7]

$$w(z) = w_0 \left[1 + \left(\frac{cz}{\pi w_0^2 \nu} \right)^2 \right]^{1/2}$$

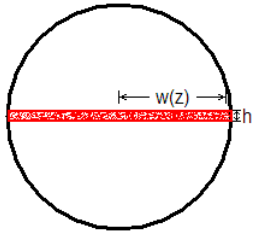


Figure 11: The geometrical model used for the fill factor assumes that the viewing area is a circle of radius $w(z)$ and the plasma is a rectangle of width $2w(z)$ and height h .

where z is the distance from the radiometer to the region being measured, w_0 is the beam waist at the antenna horn, and ν is the radiation frequency. The half-width describes the distance from the center of the field of view where the beam's irradiance drops to $1/e^2$ of its maximum value.

Evaluating the areas gives the expression

$$\begin{aligned} F &= \frac{h \cdot 2w(z)}{\pi[w(z)]^2} \\ &= \frac{2h}{\pi w(z)} \end{aligned} \quad (4)$$

where h is the height of the plasma rectangle, and the width of the rectangle is the circle's diameter ($2w(z)$). We assume a rectangle height of $h = 3$ cm. The case for $h = 1$ cm was evaluated as well. In the expression for $w(z)$, we assume the distance from the radiometer to the plasma is $z = 2$ m; changing this value to other positions along the field line doesn't significantly change the results.

After previous calculations convert the data from volts to eV, we attempt to correct for the fill factor by dividing the signal by the fill factor. (Again, consider the case where the 100 keV signal fills 10% of the view, giving an apparent signal of 10 keV. By dividing this by the fill factor, $F = 0.10$, the signal correctly becomes 100 keV.) However, this is not completely correct. If the signal was only viewed directly, with no reflections, it would be proper to simply divide by the fill factor. But if there are reflections, they should not be divided by the fill factor; reflections would fill the field of view.

Only the portion of the signal in direct view should be divided by the fill factor. To do this, we split the signal into two parts: the part in direct view and the part from reflections (both of which can be expressed as percentages of the total signal). If P_D is the percent of the signal that is in direct view, S_{raw} is the raw signal in eV, and S_{final} is the signal after account-

ing for the fill factor, then

$$S_{\text{final}} = \frac{P_D}{F} S_{\text{raw}} + (1 - P_D) S_{\text{raw}} \\ = \left[1 + P_D \left(\frac{1}{F} - 1 \right) \right] S_{\text{raw}} \quad (5)$$

This method only divides the portion of the signal in direct view ($P_D S_{\text{raw}}$) by the fill factor (F), leaving the portion from reflections ($(1 - P_D) S_{\text{raw}}$) unchanged. Note that if we let $P_D = 0$, this will leave the data unaffected by the fill factor ($S_{\text{final}} = S_{\text{raw}}$).

Treating the data in this way is separate from the definition of Case 4, which uses reflectivity factors r_1 and r_2 for the contributions of reflections. The r_1 and r_2 factors do not state how much of the emission is from direct view and how much is from reflections. However, it is possible to compare the magnitude of the total theoretical emission (Case 4) with the direct view emission (Case 3) and the emission from reflections ($r_1 \times (\text{Case 1} - \text{Case 2}) + r_2 \times \text{Case 2}$). Doing so shows that the 110 GHz emission in direct view is between 36.0% and 38.5% of

the total emission from $T = 3$ keV to 300 keV, for $r_1 = 0.10$ and $r_2 = 0.90$. But for 137 GHz emission, the percentage in direct view varies from 8.1% at $T = 3$ keV to 36.5% at $T = 300$ keV. Furthermore, these percentages vary depending on what values are chosen for r_1 and r_2 .

Although this shows that it may not be proper to apply a single P_D factor to the data across all temperatures, it is informative to see how the data changes under different assumptions. Figure 12 shows a plot with the data from shot 100804022 treated for different assumptions of P_D . The top blue curve does not treat the data for the fill factor, using the direct view model to convert ratio to temperature. The rest of the curves use the Case 4 model with reflectivity factors $r_1 = 0.10$ and $r_2 = 0.90$. The green curve below the top blue curve starts with $P_D = 0$; this is the curve that does not account for the fill factor. The temperature curve drops as P_D increases. Note that the curves spread out when $P_D < 0.50$. For large values of P_D , the curves do not vary much from the curve that assumes that the emission is all from di-

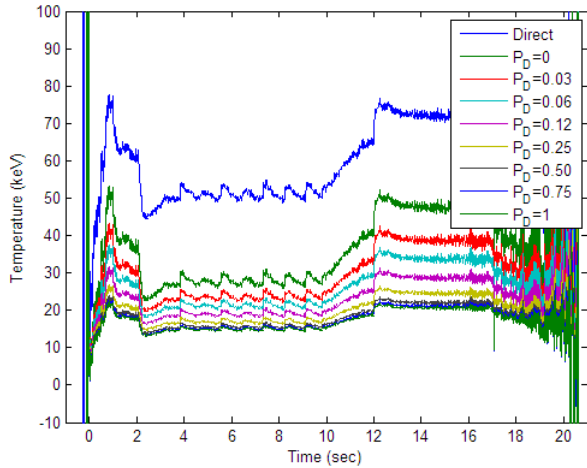


Figure 12: Several different analyses of shot 100804022, assuming $h = 3$ cm. The top blue curve uses the direct view model and no fill factor. The remaining curves, from top to bottom, use increasing values of P_D to treat the data for the fill factor.

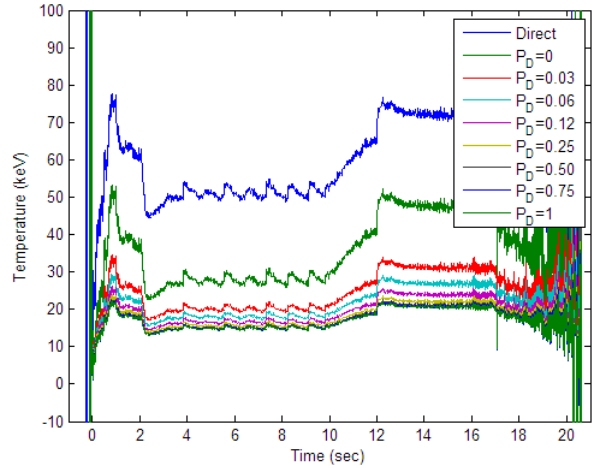


Figure 13: Several different analyses of shot 100804022, assuming $h = 1$ cm. The top blue curve uses the direct view model and no fill factor. The remaining curves, from top to bottom, use increasing values of P_D to treat the data for the fill factor.

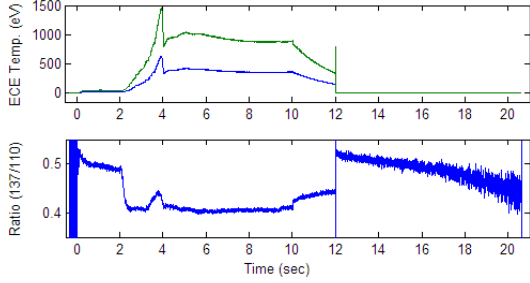


Figure 14: Data from shot 100806003. The F-coil dropped from $t = 3$ sec to 4 sec, afterward settling down in its dropped position.

rect view ($P_D = 1$). These curves vary with h as well. Figure 13 shows the same plot, except with $h = 1$ cm. The curves for $P_D = 0$ and $P_D = 1$ are the same, but the curves for intermediate values of P_D move closer to the $P_D = 1$ curve.

Modeling: another view, dropped F-coil

During the most recent experimental campaign (August 4-6, 2010), in shots 100806003 and 100806005 with helium gas, the F-coil was accidentally dropped to 22 cm below its normal position. When this occurred, the ECE signal spiked up to 1500 eV for the 110 GHz signal in shot 100806003, and up to 1700 eV in shot 100806005. In most previous shots, the signal rarely approached 1000 eV. In addition, while the F-coil was dropping, the ratio abruptly spiked up from about 0.41 to 0.44, and then quickly returned to its original value near 0.41. (See Figure 14.)

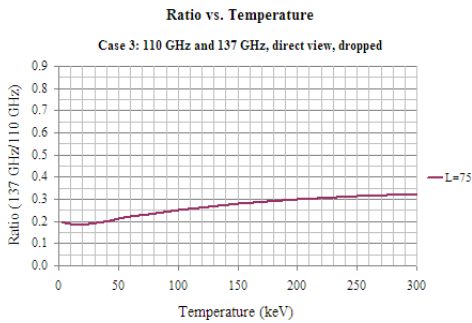


Figure 15: Calibration curve for Case 3, direct view with no reflections, $L = 75$ cm, for the case where the F-coil has dropped 22 cm.

Taking advantage of this opportunity to examine the ECE from another point of view, we modified the original MATLAB program for direct view to check what would happen when the field line drops by 22 cm. The original program specifies the location of the radiometer in R and Z coordinates; its original Z coordinate was 30.5 cm. Instead of changing the coordinates of points along the field line, we raised the coordinate of the radiometer by 22 cm to $Z = 52.5$ cm. Running this modified direct view program for many different temperatures gave a curve of ratio vs. temperature; see Figure 15.

Strictly speaking, this model is not fully correct. The F-coil dropped because the L-coil turned off. While it was turning off, the L-coil's contribution to the magnetic field in LDX dropped to zero. In addition, as the F-coil was dropping, its field followed along with it. However, once the F-coil landed in its final position, it reached a new steady state position. In this final dropped state, the L-coil was turned off, so the magnetic field surrounding the F-coil no longer contained any contributions from the L-coil; the field was only due to the F-coil. The field line that our model examines is very near to the F-coil. In both its standard position and its dropped position, the field at this location is dominated by the field of the F-coil. Therefore, although the overall field changed in a complicated way during the drop, the field line we are examining did not change significantly from its initial state after the drop.

This model suggests that the ratio would drop dramatically if the radiometer was moved to $Z = 52.5$ cm (or, equivalently, if the F-coil was dropped 22 cm). The ratio stays below 0.35 as $T \rightarrow 300$ keV in this model, yet the experimental ratio is around 0.40. In the direct view model for the F-coil in its proper position, a ratio of 0.40 indicates a temperature of 50 keV (see Figure 5). The model for the dropped F-coil indicates that the ratio would drop to around 0.22 at a tempera-

ture of 50 keV. However, the ratio remained the same, at around 0.40; if this were the case, the model suggests that the temperature suddenly increased to well over 300 keV, which is unreasonable. We find more reasonable conclusions by accounting for reflections. Using our earlier values of $r_1 = 0.10$ and $r_2 = 0.90$ for the non-dropped case, the temperature at a ratio of 0.40 is about 25 keV (see Figure 8). Using a model equivalent to Equation (2) for the dropped case, plugging in $r_1 = 0.06$ and $r_2 = 0.90$, the relationship is maintained; a ratio of 0.40 indicates a temperature of 25 keV.

Conclusions

In short, the work here shows the effect of ECE reflections on hot electron temperature. Adding reflections raises the theoretical curve of ratio versus temperature (Figure 8) and decreases the temperature that this model attributes to the hot electrons (Figure 10). Additionally, accounting for the fill factor of the plasma further decreases the temperature (Figure 12). Although we have shown that these changes drop the temperature, there remain too many unknowns to definitively state a value for the hot electron temperature. We do not know the exact L -value of the plasma; the values for r_1 and r_2 in Equation (2); or the best values to use for h and z in Equation (4) and P_D in Equation (5). Despite this, using estimated values, there is a significant decrease of the hot electron temperature. Figures 10, 12, and 13 show possible temperature ranges for different shots;

with various assumptions on parameters (r_1 , r_2 , and P_D), the hot electron temperature may lie between 15 and 50 keV. Future work will determine a more accurate range of hot electron temperature.

Acknowledgements

Support for the first author was provided by the National Undergraduate Fellowship program, administered by the Princeton Plasma Physics Laboratory and funded by the Department of Energy.

References

1. J. Kesner *et al.*, Nucl. Fusion **44**, 193 (2004).
2. A. Boxer, Ph.D. thesis, Massachusetts Institute of Technology, 2008.
3. F.F. Chen, *Introduction to Plasma Physics and Controlled Fusion*, 2nd ed. (Springer, 1984), Vol. 1, p. 20.
4. D.T. Garnier *et al.*, Phys. Plasmas **13**, 056111-1 (2006).
5. A. Nassri and M. Heindler, Phys. Fluids **31**, 95 (1988).
6. P.P. Woskov *et al.*, "Millimeter-Wave Radiometer Diagnostics of Harmonic Electron Cyclotron Emission in the Levitated Dipole Experiment (LDX)" (to be published).
7. E. Hecht, *Optics*, 4th ed. (Addison Wesley, 2002), p. 595.